ELSEVIER

Biochemical Pharmacology 64 (2002) 413–424

Biochemical Pharmacology

Cell culture model for acetaminophen-induced hepatocyte death *in vivo*

Robert H. Pierce[a], Christopher C. Franklin[b], Jean S. Campbell[b], Robert P. Tonge[c,1], Weichao Chen[c,2], Nelson Fausto[b], Sidney D. Nelson[c], Sam A. Bruschi[c,*]

[a]*Department of Pathology and Laboratory Medicine, University of Rochester School of Medicine and Dentistry, Rochester, NY, USA*
[b]*Department of Pathology, University of Washington, Seattle, WA 98195-7610, USA*
[c]*Department of Medicinal Chemistry, University of Washington, Seattle, WA 98195-7610, USA*

Received 4 June 2001; accepted 15 February 2002

Abstract

Overdose of the popular, and relatively safe, analgesic acetaminophen (*N*-acetyl-*p*-aminophenol, APAP, paracetamol) can produce a fatal centrilobular liver injury. APAP-induced cell death was investigated in a differentiated, transforming growth factor α (TGFα)-overexpressing, hepatocyte cell line and found to occur at concentrations, and over time frames, relevant to clinical overdose situations. Coordinated multiorganellar collapse was evident during APAP-induced cytotoxicity with widespread, yet selective, protein degradation events *in vitro*. Cellular proteasomal activity was inhibited with APAP treatment but not with the comparatively nonhepatotoxic APAP regioisomer, *N*-acetyl-*m*-aminophenol (AMAP). Low concentrations of the proteasome-directed inhibitor MG132 (*N*-carbobenzoxyl-Leu-Leu-Leucinal) increased chromatin condensation and cellular stress responses preferentially in AMAP-treated cultures, suggesting a contribution of the proteasome in APAP- but not AMAP-mediated cell death. APAP-specific alterations to mitochondria were observed morphologically with evidence of mitochondrial proliferation *in vitro*. Biochemical alterations to cellular proteolytic events were also found *in vivo*, including APAP- or AMAP-mediated inhibition of caspase-3 processing. These results indicate that, although retaining some attributes of apoptosis, both APAP- and AMAP-mediated cell death have additional distinctive features consistent with longer term necrosis.

Keywords: Acetaminophen; Necrosis; Apoptosis; Caspase-independent; Proteasome

1. Introduction

The general availability and widespread use of the analgesic APAP contribute to the frequency of its inadvertent or deliberate overdose. As a result, overdose from APAP constitutes a public health problem despite its relative safety when administered appropriately. The liver damage manifests as a localized centrilobular cell death that can be fatal [1]. Treatment options for such overdose victims are limited after 12–24 hr post-ingestion, due, in part, to gaps in our understanding of the mechanism by which APAP produces hepatotoxicity. The structural isomer of APAP, AMAP, has analgesic properties [2] and is currently under development as an alternative to APAP. Although considered safer due to the lack of observable hepatotoxic effects [3,4], AMAP nonetheless has the potential to add to this public health problem.

Despite elegant pioneering studies [5], and subsequent efforts (for recent reviews see Refs. [6–8]), many aspects of the cell biology of APAP-mediated hepatotoxicity remain

* Corresponding author. Tel.: +1-206-543-7360; fax: +1-206-685-3252.
E-mail address: sambru@u.washington.edu (S.A. Bruschi).
[1] Current address: AstraZeneca, Alderly Park, Macclesfield, Cheshire SK10 4TG, England, UK.
[2] Current address: Pfizer Central Research, Groton, CT 06340, USA.

Abbreviations: AMAP, *N*-acetyl-*m*-aminophenol; APAP, *N*-acetyl-*p*-aminophenol, acetaminophen, paracetamol; APAP–GSH, glutathione conjugate of acetaminophen; ATF3, activating transcription factor 3; CAD/DFF40, caspase-activated deoxyribonuclease/DNA fragmentation factor 40 kDa; CHEF, clamped homogeneous electric field; CYP, cytochrome P450; Cyp2e1, murine homologue of human CYP2E1; Cyp3a, murine homologue of human CYP3A4; DAPI, 4,6-diamino-2-phenylindole; Ac-DEVD-amc, acetyl-Asp-Glu-Val-Asp-aminomethylcoumarin; ER, endoplasmic reticulum; *GADD153*, growth arrest and DNA damage inducible gene; ICAD/DFF45, inhibitor of caspase-activated deoxyribonuclease/DNA fragmentation factor 45 kDa; Ac-LEHD-amc, acetyl-Leu-Glu-His-Asp-aminomethylcoumarin; z-LLL-amc, *N*-benzyloxycarbonyl-Leu-Leu-Leucinal-aminomethylcoumarin; NAPQI, *N*-acetyl-*p*-benzoquinone imine; PARP, poly(ADP-ribose) polymerase; TGFα, transforming growth factor α; TNFα, tumor necrosis factor α; and Ac-VEID-amc, acetyl-Val-Glu-Ile-Asp-aminomethylcoumarin.

0006-2952/02/$ – see front matter
PII: S0006-2952(02)01180-2

unknown. Bioactivation of APAP in the endoplasmic reticulum, predominantly by CYP2E1 [9,10], results in the formation of NAPQI, the major reactive metabolite responsible for covalent modification of cellular target proteins, cell death, and organ damage [10,11]. Although the identities of many target proteins arylated by NAPQI have now been established in the mouse model [8,12], no clear links between these modifications and resultant cell death are evident. Other important facets of APAP-induced cytotoxicity have also been investigated over the years, including the contribution of total cellular and organellar thiol levels [13–15], mobilizations of intracellular calcium stores [16–18], and cellular redox alterations (e.g. lipid peroxidation [19–21]). Complex interrelationships exist between these biochemical perturbations and the subsequent onset of cytotoxicity (for reviews see Refs. [6,7,22]). Any semblance of agreement in the past regarding the progression of cellular injury by APAP has been placed into question more recently with several counterintuitive *in vivo* studies [21,23–25]. To address these anomalous findings for APAP-induced hepatotoxicity in transgenic animal systems, we recently proposed a scheme that links organ damage to the cellular capacities to remove adducted and transgenically overexpressed proteins [7].

In the present work, an *in vitro* system for aspects of APAP-mediated cell death has been established which closely models several clinical criteria for this form of hepatotoxicity. In particular, we have focused on the characteristics of cell damage that may provide further insight into the mode of cell death induced by APAP. We report here partial characterizations of this culture model and a distinctive form of cell death following APAP treatment with some similarities to apoptosis but also with unexpected necrotic elements.

2. Materials and methods

2.1. Reagents

Unless otherwise indicated, all chemicals were obtained from the Sigma Chemical Co.

2.2. Cell culture conditions

Serum-free culture of the TAMH cell line, passages 19–40, was as previously described [26]. Briefly, growth and passage of cells were in serum-free Dulbecco's modified Eagle's medium/Ham's F12 (Gibco) supplemented with 5 μg/mL of insulin, 5 μg/mL of transferrin, 5 ng/mL of selenium (Collaborative Biomedical Products), and 0.1 μmol/L of dexamethasone, 10 mM nicotinamide, and 50 μg/mL of gentamicin. Cultures were maintained in a humidified incubator with 5% carbon dioxide/95% air atmosphere and passaged when 70–90% confluent (approx. 5–7 days). To avoid potential complications associated with solvent vehicle, the stock solutions for *in vivo* and TAMH culture dosing were prepared by directly sonicating APAP or AMAP into aqueous solution using an ultrasonic probe tip (10 × stock in culture medium or 30 mg/mL in PBS, respectively; Series 4710 Ultrasonic Homogenizer, Cole-Palmer) followed by 0.22 μm filter sterilization (Steriflip, Millipore). To initiate apoptosis, TAMH cultures were pretreated with actinomycin D (200 nM, 30 min) followed by TNFα (20 ng/mL; R&D Systems).

2.3. Cell viability determinations

Cellular viability was assessed by a Live/Dead® Cytotoxicity Kit (Molecular Probes) based on intracellular esterase formation of calcein from cell permeant calcein-acetoxymethyl ester or nuclear entry of impermeant ethidium homodimer. Assay procedures were conducted exactly as described by the manufacturer.

2.4. In vitro glutathione conjugate formation

Cell culture supernatants were deproteinized with 3% (w/v) sulfosalicylic acid prior to HPLC analysis on a Hewlett-Packard 1090 II/L system with a Hewlett-Packard 1049A electrochemical detector (Hewlett-Packard). The glutathione conjugate of APAP (APAP–GSH) was subsequently determined exactly as previously described with separations performed on a 3.5-mm Zorbax SB-C_{18} column (4.6 mm × 15 cm) using a mobile phase of 25 mM ammonium phosphate buffer containing 10% (v/v) methanol and 0.2% (w/v) acetic acid [11].

2.5. Determination of nuclear morphology

Trypsinized TAMH cultures were washed, fixed in 70% ethanol, and stored at −20° prior to subsequent analysis. Chromatin morphology was assessed by staining cell pellets with DAPI [2.5 mg/mL final concentration in 10% (v/v) DMSO, Molecular Probes] and were visualized by UV-excitable fluorescence microscopy.

2.6. Chromosomal DNA analysis by CHEF gel electrophoresis

Adherent cells from control and treated TAMH cultures were trypsinized, pooled with nonadherent cells, washed, and embedded in 1.5% low melting point (LMP) agarose (SeaPlaque®, FMC). Gel blocks were soaked in nuclei lysis buffer (10 mM Tris–HCl, pH 6.0, 100 mM EDTA, 20 mM NaCl, 20 mg/mL of proteinase K, 1% lauroylsarcosine) for 20 hr at 50° and then washed and stored at 4° in 10 mM Tris–Cl, 1 mM EDTA (pH 8.0). Blocks were transferred into the wells of a horizontal 1% agarose gel (SeaKem® Gold, FMC) and sealed in place with additional LMP agarose. CHEF electrophoresis was performed

using a CHEF system (Bio-Rad model 200/2.0 supply and a pulsewave 760 switcher) and gels were run at 20° and 200 V for 20 hr with a pulse ramp of 0.2–22 sec prior to staining with ethidium bromide. Bacteriophage λ concatamers were used as molecular weight markers.

2.7. Determination of caspase and proteasome activities

Caspase activities were determined as previously described [27]. Briefly, soluble protein (50 μg) from whole cell lysates was incubated for 30 min at 37° in 100 μL of caspase assay buffer [50 mM HEPES, pH 7.4, 100 mM NaCl, 2 mM EDTA, 20% sucrose (w/v), 0.2% (w/v) CHAPS {3-([3-cholamidopropyl]dimethylammonio)-1-propanesulfonate}] containing 20 μM Ac-DEVD-amc (caspase-3/7; Alexis Biochemicals), Ac-VEID-amc (caspase-6; Calbiochem), or Ac-LEHD-amc (caspase-9; Bachem), and fluorescence was monitored on a Packard Fluorocount microplate fluorometer with an excitation wavelength of 360 nm and an emission wavelength of 460 nm. Substrate autofluorescence was subtracted from each value, and data are presented as fold activation over extracts from untreated cells. Proteasome activity was measured in an identical manner utilizing the fluorescent substrate z-LLL-amc (Calbiochem) exactly as previously described [28].

2.8. Electron microscopy

Adherent and nonadherent hepatocytes from control, 5 mM APAP-, or 5 mM AMAP-treated TAMH cultures were fixed using Karnovsky's fixative (1/2 strength glutaraldehye–formaldehyde), embedded, and stained with uranyl acetate and Reynold's lead citrate. Specimens were examined using a Philips 410 Transmission Electron Microscope.

2.9. Isolation of subcellular fractions and immunoblotting procedures

Subcellular fractions were prepared by standard procedures from $B6C3F_1$ (see Fig. 7) or Swiss–Webster (data not presented) mice receiving 500 mg/kg (i.p.) APAP, AMAP, or saline vehicle at 2 and/or 4 hr after dosing exactly as previously described [9]. The relative purity of subcellular fractions was assessed by monitoring lactate dehydrogenase (cytosol) and succinate cytochrome *c* reductase (mitochondria) marker enzyme activities exactly as previously described [9]. Cytosolic contamination of mitochondrial preparations ranged from 0 to 9.8%, whereas contamination of cytosolic fractions with mitochondria ranged from 1.1 to 12.5%. Protein samples (subcellular fractions or total TAMH cell lysates) were loaded at 50 μg/lane and resolved on 10–15% SDS–PAGE minigels (Mini-Protean, II, Bio-Rad) and transferred to nitrocellulose (1 hr, 15 V, Trans-Blot SD Semi-Dry Transfer Cell, Bio-Rad). Immunodetection was by chemiluminescence (SuperSignal® ULTRA, Pierce) using antibodies to ATF3, GADD153 (Santa Cruz Biotechnology), PARP (purchased from G.G. Poirier), caspase-3 (D.W. Nicholson), and ICAD (W. Earnshaw and K. Samejima).

3. Results

3.1. Clinically relevant concentrations for in vitro bioactivation and cell death by APAP

The cytotoxicities of APAP and AMAP were assessed *in vitro* using a transgenic murine hepatocyte cell line (TAMH), which has been shown previously to maintain a differentiated phenotype irrespective of passage [26]. Comprehensive characterizations of transgenic TGFα overexpression in TAMH and related cell lines have been reported previously [26,29]. TAMH cultures exposed to increasing concentrations of APAP were found to undergo cytoplasmic retraction and cell lifting reminiscent of apoptosis (Fig. 1A). Similar, but not identical, cell-shrinkage alterations also were observed with AMAP but at high concentrations only (Fig. 1A, right panel). An assessment of the plasma membrane integrity of treated cultures with fluorescent vital dyes nonetheless confirmed late (48–72 hr) disruptions of the plasma membrane consistent with a secondary necrosis phenomenon induced by either APAP or AMAP *in vitro* (Fig. 1B).

Evidence for cell death via the formation of the NAPQI reactive intermediate, most likely by endogenous CYP monooxygenase activity(ies), was provided by the detection of the APAP–GSH conjugate (Fig. 1C). The APAP–GSH product is generally considered a product of sequential Phase 1 and 2 metabolism and was observed in the culture medium even with relatively low concentrations of APAP (i.e. 1 mM) and increased markedly with 10 mM APAP treatment, indicating a dose-related production of NAPQI *in situ* (Fig. 1C). We have estimated that the rate of APAP–GSH formation in TAMH cultures is equivalent to 36–108 nmol/liver/hr with a 1 mM APAP dose or 56–168 nmol/liver/hr with 10 mM APAP ($2–6 \times 10^7$ hepatocytes/0.75 g liver [wet weight] of a young adult mouse; N. Fausto, unpublished observation). This compares favorably with the literature, which indicates APAP–GSH formation in mouse liver of approx. 10 nmol/liver/hr after an APAP dose of 250 mg/kg [30] or approx. 30–60 nmol/liver/hr after 500 mg/kg [31]. Finally, a quantitative comparison of the cytotoxic potential of APAP and AMAP confirmed that the AMAP positional isomer was considerably less cytotoxic in agreement with previous *in vivo* studies (Fig. 1D; [15,18]).

3.2. APAP- and AMAP-induced alterations to TAMH nuclear morphology

Morphological alterations to TAMH nuclei and DNA integrity were investigated both *in vitro* and *in vivo* by

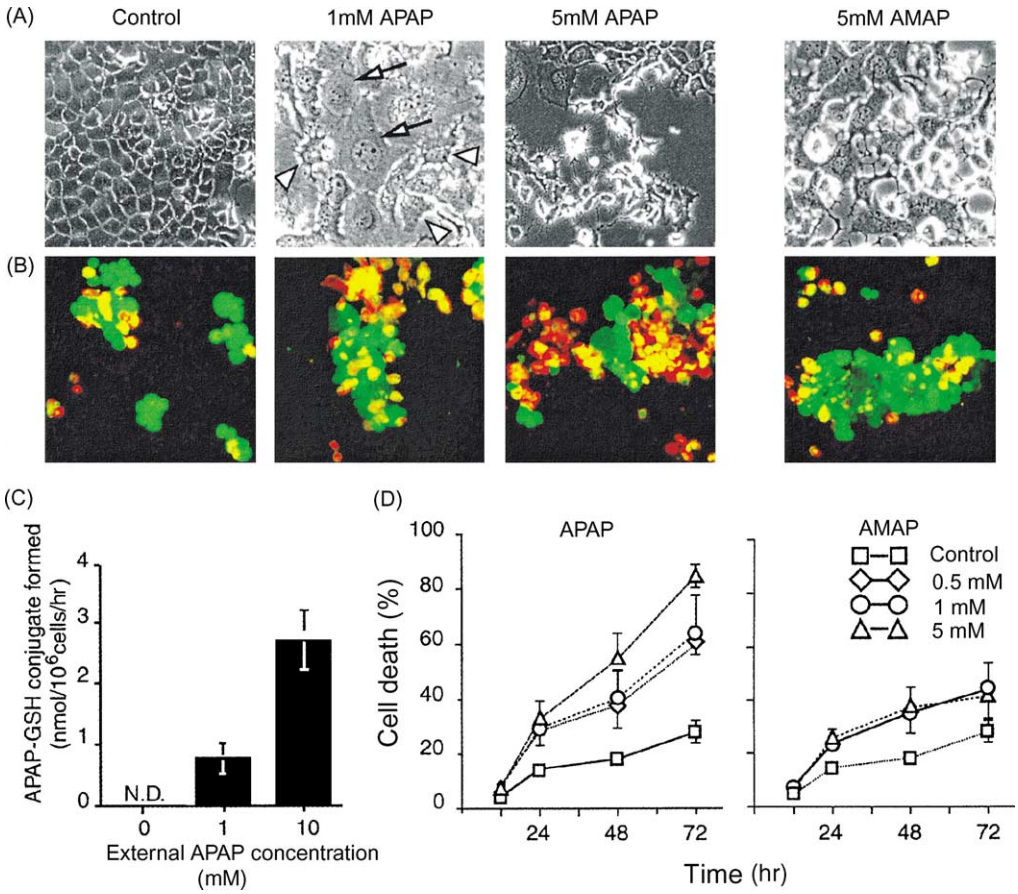

Fig. 1. Bioactivation, changes to cellular morphology, and cell death induced by APAP, and the positional isomer AMAP, in the TGFα-transgenic hepatocyte cell line, TAMH. (A) Cellular morphology by light microscopy of cultures exposed to 0 (Control), 1 and 5 mM APAP, or 5 mM AMAP for 24 hr. Progressive cytoplasmic retraction and nuclear disintegration are indicated (arrowheads) in susceptible cells from 1 mM APAP-treated cultures. Adjacent healthy cells with normal morphology are also shown (arrows). Nonadherent and dead cells were observed out of the plane of focus for all treatments and appeared as smaller, light-colored, spheres in all treatment groups. Mag. 200×(except for 1 mM APAP, 400×). (B) Representative cultures of pooled nonadherent and adherent cells, after a 72-hr exposure, assessed for viability using the Live/Dead assay® (refer to Section 2). Viable cells have a green fluorescence, whereas nonviable cells appear as red/yellow. Mag. 200×. (C) Corresponding media supernatants were analyzed for dose-related capacity to produce the reactive intermediate of APAP (NAPQI) by formation of the corresponding glutathione conjugate (APAP–GSH, refer to Section 2). (D) Dose-related cell death evident in APAP-treated cultures (left panel) but not with AMAP treatment (right panel). Data for (C) and (D) are from three or more independent determinations [means ± SEM, N = 3 (C) and N = 3–6 (D)]. Errors are less than symbol width where none are apparent.

fluorescent DAPI staining or agarose gel electrophoresis, respectively, based on previous reports indicating that APAP initiates oligosomal fragmentation [32,33].

DAPI staining indicated that APAP (0.5–5 mM) produced extensive chromatin margination and, rarely, complete condensation of TAMH nuclei (Fig. 2A, upper panels). Chromatin margination was also observed with equimolar concentrations of AMAP, although complete chromatin collapse into fully developed apoptotic bodies was not a characteristic of the nonhepatotoxic isomer (Fig. 2A, upper panels). Addition of very low concentrations of the proteasome-directed inhibitor MG132 (*N*-carbobenzoxyl-Leu-Leu-Leucinal), previously determined to have no observable effect on TAMH growth and morphology (100–250 nM, data not presented), qualitatively increased the incidence of both chromatin margination and condensation for both compounds without altering the nuclear morphology of cultures not treated with APAP or AMAP (Fig. 2A, lower panels). Consequently, these studies differ substantially from those in the current literature where far higher concentrations of MG132 (*ca.* 10–100 μM) are routinely used (e.g. Refs. [34–36]).

Differential potencies for DNA fragmentation were also evident for the two isomers by CHEF gel electrophoresis (Fig. 2B). Formation of high molecular weight DNA fragments after 36 hr of treatment were observed with as low as 1 mM APAP in contrast to AMAP-induced fragmentation which required concentrations of 10 mM (Fig. 2B). Time-dependent formation of approx. 50 kbp fragments *in vitro* by APAP, first observed at 24 hr, was consistent with the profile of cell viability loss (Figs. 1D and 2C). APAP-generated 50 kbp fragments *in vitro* (Fig. 2B and C) or *in vivo* (Fig. 2E, APAP 2 hr) appeared to comigrate well with fragments formed after dosing with actinomycin D/TNFα (act.D/TNFα) to induce apoptosis (Fig. 2D and E). Nonetheless, the onset of DNA fragmentation by act.D/TNFα was considerably

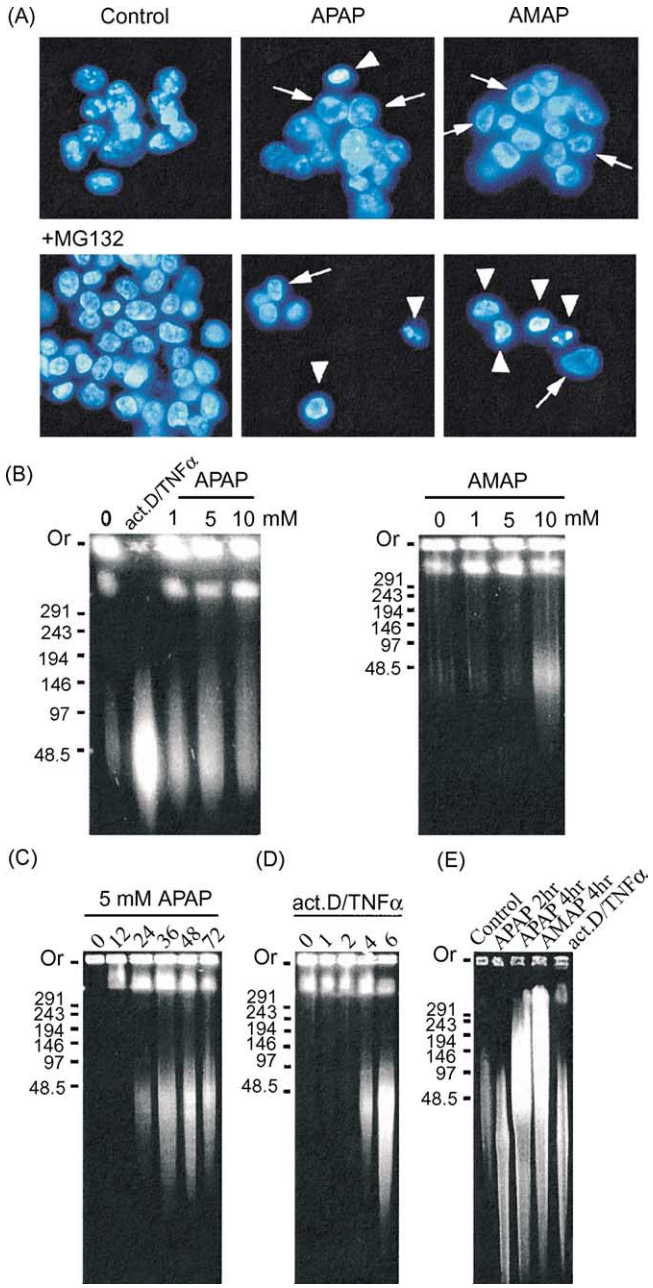

Fig. 2. Alterations to nuclear morphology and chromatin structure by APAP and AMAP and enhancement with the proteasomal inhibitor MG132. (A) Upper panels: Nuclear DAPI staining of TAMH cultures treated with 5 mM APAP or AMAP. Chromatin margination (arrows) was evident at 24 hr for both compounds although complete chromatin condensation (arrowhead) was seen only rarely in APAP-treated cultures only. Lower panels: Addition of the proteasome-directed inhibitor MG132 (250 nM) markedly increased the incidence of both chromatin margination (arrows) and condensation (arrowheads) in treated cultures without altering the normal punctate DAPI staining of control TAMH cultures. Mag. 1000×. Results are from three independent experiments, each with N = 3–5 replicate plates per treatment group. (B) Comparative potency of 50 kbp DNA fragmentation in TAMH cultures treated with either 1–10 mM APAP (left panel) or 1–10 mM AMAP (right panel) for 36 hr. AMAP- and APAP-induced 50 kbp fragments comigrated with act.D/TNFα degradation products (left panel). (C) Time course of high molecular weight DNA fragmentation (approx. 50 kbp) in TAMH cultures treated with 5 mM APAP (0–72 hr). Panels B and C show data from duplicate, independent experiments for each panel (total N = 4). (D) Time course evaluation of *ca.* 50 kbp fragment formation following act.D/TNFα treatment (0–6 hr). (E) Increased *in vivo* formation of 50 kbp and higher mass fragments by APAP and AMAP in the livers of B6C3F$_1$ mice in comparison to control animals. (Note: formation of *ca.* 300 kbp DNA fragments in AMAP-treated animals.) Material from act.D/TNFα-treated TAMH cells served as a positive control (right lane). Molecular mass of λ DNA standards, in kbp, are indicated on the left of panels B–E. Panels D and E are each representative of a single determination only.

faster than observed with APAP treatment (compare Fig. 2C with Fig. 2D). DNA fragmentation by APAP or AMAP *in vivo* resulted in even larger chromosomal fragments that ranged in size from 50 kbp up to 300 kbp (Fig. 2E). Conventional agarose gel electrophoresis was additionally used to determine the extent of oligosomal DNA fragmentation, but none was detected by this procedure either *in vitro* or *in vivo* even in the presence of considerable higher molecular mass degradation (data not presented).

3.3. Differential cellular stress activation in TAMH cultures after hepatotoxic APAP treatment in comparison to the nonhepatotoxic isomer, AMAP

Differential cellular responses to the hepatotoxic and nonhepatotoxic isomers were observed as increased protein levels of the highly stress-inducible transcription factor ATF3, a member of the CREB/ATF family (Fig. 3A; [37,38]). In addition, the downstream ATF3 target *GADD153*, a pivotal stress responsive gene [38–40], was preferentially up-regulated in response to APAP treatment and its level of expression was increased with combined AMAP/MG132 treatments (Fig. 3A, lower panel). This preferential up-regulation of GADD153 with cytotoxicity was evident for at least 12 hr following APAP or AMAP dosing (Fig. 3B).

3.4. Protein degradation and caspase activities after APAP and AMAP treatment in vitro and in vivo

The time course of APAP-induced DNA fragmentation *in vitro* was found to closely parallel the breakdown of the large splice variant of ICAD (inhibitor of caspase-activated deoxyribonuclease, ICAD-L; [41]), the murine equivalent of human DNA fragmentation factor 45 kDa (DFF45; compare Fig. 4 with Fig. 2C), and was consistent with activation of this apoptotic nuclease [41,42].

Degradation of an ER-resident CYP isoform (Cyp2e1) and nuclear PARP was also evident and both with an identical time course to that found with ICAD breakdown (Fig. 4), indicating that proteolytic degradation occurs in three disparate cellular compartments during APAP-mediated cytotoxicity. In contrast, a related Cyp3a isoform, detected with cross-reacting antisera to human CYP3A4, was not degraded in TAMH cells under the same conditions (Fig. 4).

APAP-mediated PARP degradation was coincident with progressive loss of DNA integrity and proteolytic cleavage

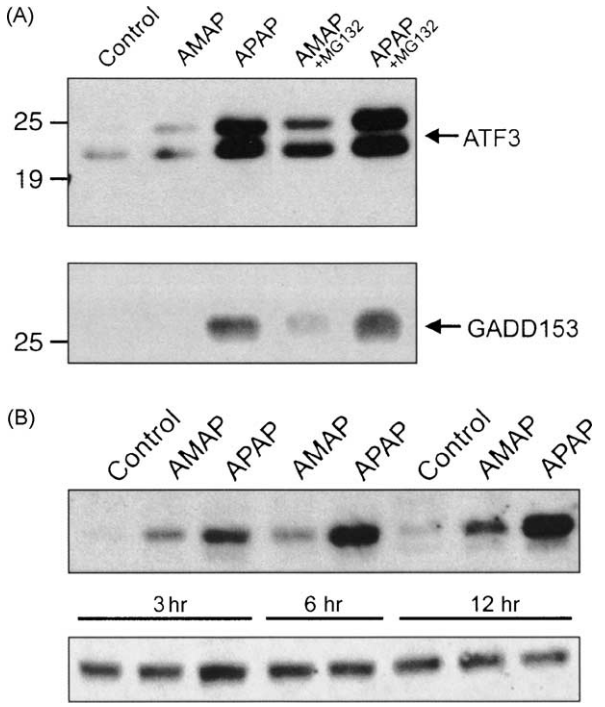

Fig. 3. Differential, ATF3-mediated, cellular stress responses to hepatotoxic APAP in comparison to non-hepatotoxic AMAP. (A) Protein levels of the stress-responsive transcription factor ATF3 (upper panel) and its target gene *GADD153* (lower panel) were determined by immunoblot analyses following a 24-hr exposure to cytotoxic (5 mM APAP) or non-cytotoxic (5 mM AMAP) treatments in either the presence or the absence of the proteasome-directed inhibitor MG132 (100 nM). Migration of molecular weight standards are shown to the left of each panel. Representative of a single independent experiment (total of N = 3). (B) Time course evaluations of GADD153 protein levels in TAMH cultures treated with APAP or AMAP (5 mM) in comparison to media vehicle controls [upper panel; representative of a single independent experiment (total of N = 3)]. Consistent loading between lanes was independently confirmed on the same blot by non-specific binding of anti-rabbit IgG antiserum (lower panel).

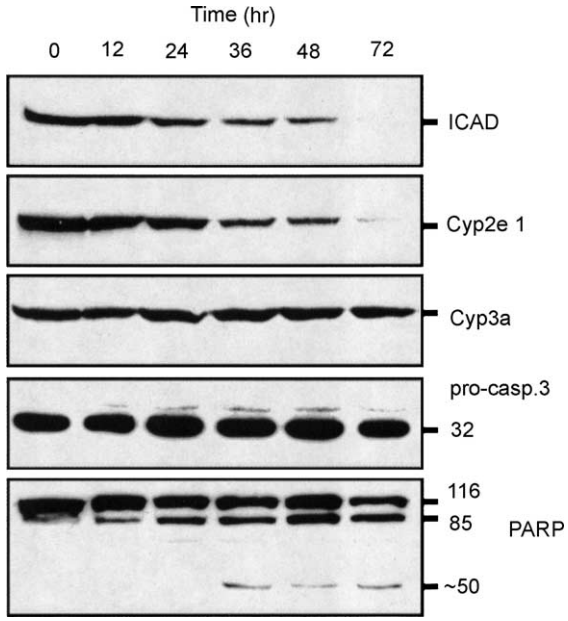

Fig. 4. APAP-mediated induction of proteolytic processing of selected proteins in TAMH cultures. Extended proteolytic degradation of only selected proteins, from differing subcellular localizations, after 5 mM APAP treatment *in vitro* (0–72 hr). Time-dependent loss from total TAMH cell lysates of ICAD-L, Cyp2e1, and PARP, with near identical kinetics, in comparison to the maintenance of intact/unprocessed procaspase-3 and a murine homologue to human CYP3A4 (Cyp3a). This figure is indicative of a single time–course experiment (N = 3 replicate plates/time point) with each panel representing an independent reprobing of the nitrocellulose filter with the antibodies shown on the right.

of ICAD over the course of TAMH cell death *in vitro* (Fig. 4). Generation of both 85 and 50 kDa fragments after APAP treatment *in vitro* was in agreement with necrotic, non-caspase-mediated, proteolytic processing of PARP as has been shown previously in necrotic HL-60 cells [43].

Selected caspase activities were assessed using tetrapeptide fluorogenic substrates during APAP-mediated TAMH cytotoxicity. Despite an absence of procaspase-3 processing by immunoblot analyses (Fig. 4), Ac-DEVD-amc cleavage was observed in TAMH cultures after APAP treatment (Fig. 5A, left panel). As both caspase-7 and caspase-3 have overlapping optimal cleavage specificities, these data may indicate caspase-7 activation in TAMH cultures and require further confirmation [44]. Nonetheless, the induction of Ac-DEVD-amc cleavage with APAP treatment was 10-fold lower than comparable activities found after treating TAMH cultures with proapoptotic act.D/TNFα (Fig. 5A, compare right and left panels).

Other potentially important caspase activities were also minimally elevated. In keeping with the modest induction of Ac-DEVD-amc cleavage activity in APAP-treated cultures, the relative induction of both caspase-6 and caspase-9 activities was small, being less than a 2-fold increase above control values (Fig. 5B, left panel). That these elevations were potentially unimportant biologically was suggested from act.D/TNFα-treated TAMH cultures where caspase-6 and caspase-9 activities increased by approximately an order of magnitude above control levels (Fig. 5B, compare right and left panels). Similarly, only marginal caspase (Ac-DEVD-amc, caspase-6 or caspase-9) activation was observed *in vivo* after APAP or AMAP treatments at early points shown previously to be important in the progression of injury (Fig. 5C; [15]).

Earlier work has shown that the only cellular protease directly arylated by NAPQI is the proteasome (specifically, the C8 subunit; [12]). Consequently, a demonstration of decreased proteasomal activity(ies) after APAP treatment may confirm it as a potentially critical site for NAPQI-mediated protein arylation and subsequent cell death. *In vitro* proteasomal chymotryptic activity was inhibited by up to 60% in APAP-, but not act.D/TNFα-treated cultures (Fig. 5B). In terms of magnitude, a comparable, but transient, inhibition of proteasomal activity was also observed after a single *in vivo* dose of APAP (50% inhibition at 2 hr, Fig. 5C).

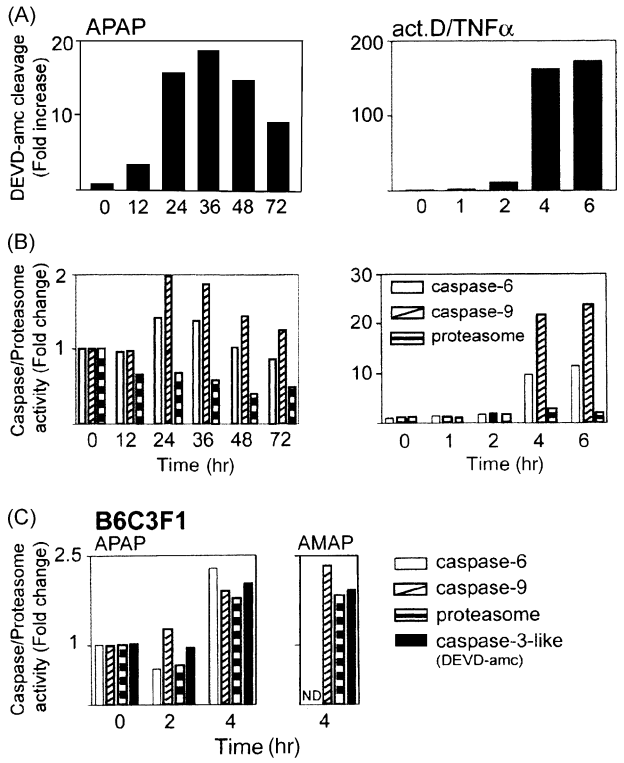

Fig. 5. Comparison of alterations in TAMH proteolytic activities after drug treatment (APAP or AMAP) or induction of apoptosis with actinomycin D/TNFα. (A) Caspase-3-like activities (DEVD-amc cleavage) in TAMH cultures treated with either 5 mM APAP (left panel) or act.D/TNFα (right panel). Activities are expressed as a fold induction from initial activity (as described in Section 2). Absolute DEVD-amc cleavage activities ranged from 0.67 to 294.7 pmol product formed/min/mg protein for control (t = 0 hr) and act.D/TNFα treatments (t = 6 hr), respectively. (B) Comparison of TAMH cellular caspase-6, caspase-9, and proteasome activities in cultures treated with either 5 mM APAP (left panel) or act.D/TNFα (right panel) and expressed as fold induction from initial activity. Proteolytic activities, in pmol/min/mg protein, ranged as follows: caspase-6 (88.3 to 146.8 for APAP; 22.6 to 262.6 for act.D/TNFα), caspase-9 (6.1 to 13.7 for APAP; 1.6 to 51.2 for act.D/TNFα), and the proteasome (11.9 to 30.6 for APAP; 5.9 to 17.4 for act.D/TNFα). (C) Comparison of hepatic caspase and proteasomal activities in B6C3F_1 mice after APAP or AMAP administration (600 mg/kg, i.p.). Proteolytic activities, expressed as pmol/min/mg protein, ranged as follows: caspase-3-like (0.3–2.99), caspase-6 (2.02–9.5), caspase-9 (0.57–2.1), and the proteasome (0.65–2.86). Data are presented as averages from one of two independent experiments with replicate plates or animals for each experiment. ND = not determined.

3.5. Alterations to cellular morphology following in vitro APAP and AMAP treatments

Electron micrographs of TAMH cultures confirmed the selective toxicity of APAP to the mitochondrion. In particular, an early proliferation (<12 hr) of electron dense mitochondria was apparent with APAP treatment (Fig. 6) in agreement with our previous *in vivo* results showing similarly altered mitochondria [25]. Nonetheless, mitochondrial proliferation after APAP treatment in TAMH cultures was qualitatively variable between individual cells (Fig. 6; e.g. APAP, 48 hr). APAP-induced mitochondrial proliferation was also associated with other functional deficits to this organelle, including a dose-related collapse of the inner mitochondrial membrane potential (data not shown). Although mitochondrial proliferation was not observed with AMAP treatment, the nonhepatotoxic isomer still produced delayed effects (48–72 hr) on this organelle by increasing both electron density and overall size (Fig. 6). A substantial proliferation of the rough ER was a distinctive attribute of AMAP treatment in TAMH cells that was not observed with APAP exposure (Fig. 6).

3.6. Proteolytic and apoptotic-like cellular alterations associated with in vivo APAP and AMAP treatments

The cleavage of effector caspase substrates was examined in hepatic subcellular fractions as a correlate to the *in vitro* data. We observed that nuclear PARP, a known caspase-3 substrate, was not cleaved following APAP treatment *in vivo* and remained at the native size (Fig. 7). PARP cleavage was evident with AMAP treatment, however, to fragment sizes previously associated with necrosis (56 and 52 kDa) and not caspase-directed apoptosis [43]. A redistribution of native ICAD was observed into the nucleus, with either APAP or AMAP treatment, suggesting cotransportation of both ICAD and CAD into this compartment (Fig. 7).

In the cytosol, caspase-3 was observed as both the 32 kDa proenzyme and a minor 20 kDa precursor form in untreated hepatic tissue (Fig. 7). In comparison, the procaspase-3 form at 32 kDa was predominant in APAP-treated tissue at 2 hr. At the 4-hr treatment, however, only the 32 kDa form was found in either APAP- or AMAP-treated tissues with a complete absence of the 20 kDa form even with extended film exposures (Fig. 7). Nonetheless, we have shown previously substantial increases in hepatic proteolysis and early proapoptotic BAX-associated release of mitochondrial cytochrome *c* into the cytosol with *in vivo* APAP, but not AMAP, treatments [25].

4. Discussion

In vitro methodologies that adequately model the molecular and cellular characteristics of APAP-induced hepatocyte death *in situ* have been elusive. Many studies have focused on primary hepatocyte/organ cultures (either rodent or human) or, more recently, human hepatocyte lines transfected with and overexpressing CYP isozymes [45,46]. These model systems have generally required high APAP concentrations to instigate cytotoxicity, typically in excess of the plasma APAP levels observed clinically. *In vitro* mechanistic studies with APAP have generally been conducted in the 5.0–10.0 mM range as this is the concentration where cytotoxicity first becomes evident. In contrast, the clinical evidence indicates that early plasma APAP levels are almost always at least 5-fold lower (i.e. 1.0–2.0 mM) during APAP poisoning in humans

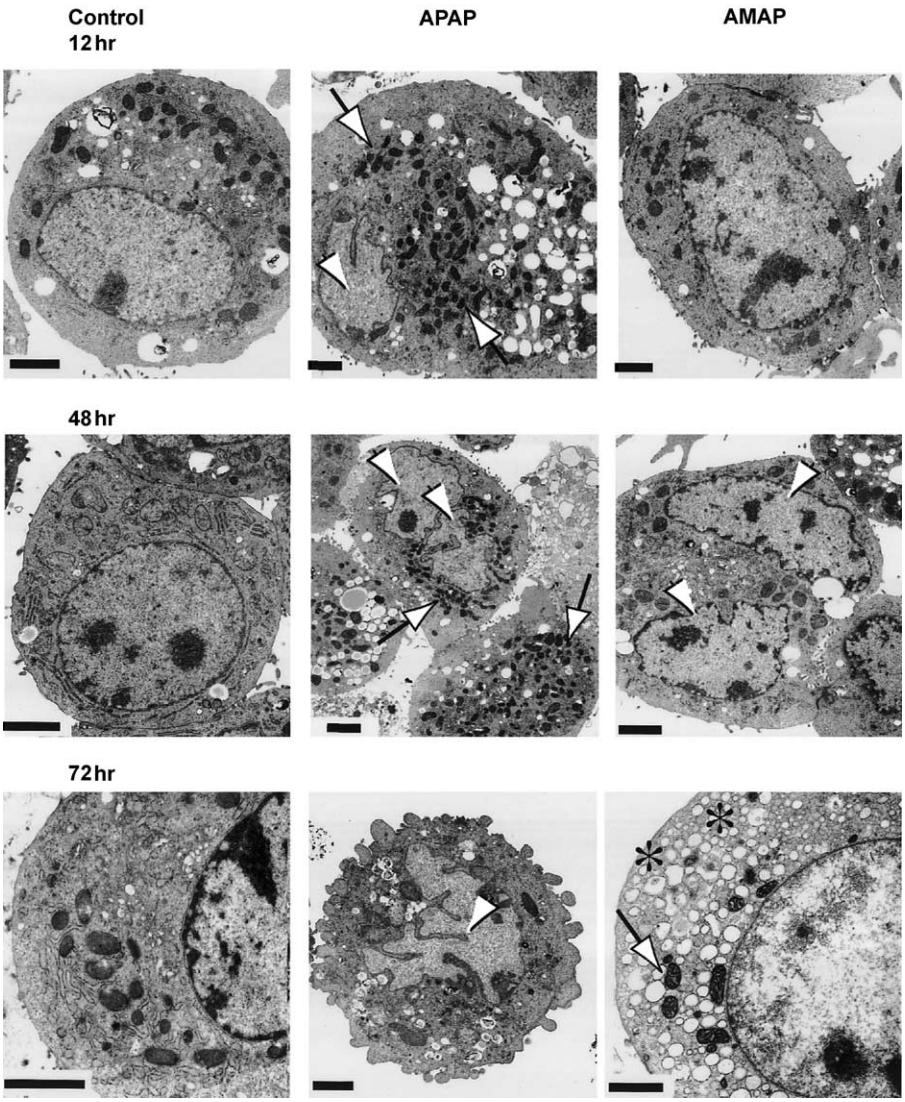

Fig. 6. Time course assessment of TAMH morphology by electron microscopy following treatment with APAP and AMAP. Assessment of TAMH morphology by electron microscopy indicating proliferation of electron dense mitochondria (arrows) and nuclear degradation (arrowheads) as early as 12 hr after treatment with 5 mM APAP (APAP) in comparison to untreated cultures (Control). Mitochondrial proliferation was not evident in 5 mM AMAP-treated cultures (AMAP) although slight alterations to nuclear morphology were observed (arrowheads). After a 72-hr exposure, APAP-treated cultures were in advanced decay, whereas electron dense mitochondria with dilated cristae (arrow) and considerable proliferation of the rough ER (*) were found in the surviving fraction of AMAP-treated cultures. Bar represents two microns. Shown are representative micrographs from a single time–course experiment with either duplicate or triplicate plates for each time point.

[1]. Consequently, as the mechanism of cytotoxicity is likely to differ at high concentrations, the development of an appropriate *in vitro* model for APAP-mediated cell death is still of importance.

Initially, we examined APAP-induced cytotoxicity in the TAMH cell line, which, as a result of TGFα overexpression, maintains an invariant differentiated phenotype *in vitro* [26]. To establish the utility of this cell culture system for APAP bioactivation, we confirmed that TAMH cultures express, in a passage-independent manner (Fig. 4 and data not presented), the two murine cytochrome P450 isozymes homologous to human CYP2E1 and CYP3A4 that are known to activate APAP and AMAP [47]. Endogenous CYP expression resulted in dose-related formation of a "downstream" metabolic product (APAP–GSH) providing good evidence for cellular bioactivation of APAP via production of the protein damaging species, NAPQI (Fig. 1C). Further inhibitor studies will be necessary, however, to definitively confirm the exact contributions of various CYP isozymes to NAPQI production and subsequent TAMH cell death.

In contrast to the published literature, we have observed significant TAMH cytotoxicities and DNA fragmentation at comparatively low APAP doses (0.5–1.0 mM) in good agreement with plasma APAP levels found in human overdose scenarios [1]. Although altered TAMH cellular morphologies, e.g. cytoplasmic retraction and chromatin condensation, would appear to be suggestive of cell death

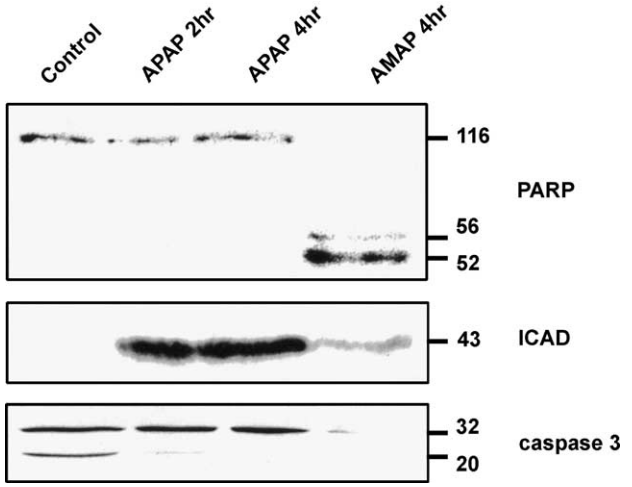

Fig. 7. Biochemical alterations induced by APAP and the nonhepatotoxic positional isomer, AMAP, *in vivo*. Subcellular fractions from B6C3F$_1$ mice were isolated at various times after APAP or AMAP treatment (500 mg/kg, i.p.) and immunoblotted using standard procedures. Upper panels: Nuclear samples indicating the absence of PARP cleavage in APAP-treated animals but with necrotic-like degradation of PARP in AMAP-treated samples in comparison to saline vehicle-treated samples (Control, top panel). Migration of native ICAD into the nucleus was observed in all treatment groups (middle panel). Bottom panel: Cytosolic fractions immunoblotted for the presence of (pro-)caspase 3 indicating suppression of basal procaspase-3 processing in all treatment groups. Molecular mass of immunoreactive proteins, in kDa, is indicated on the right of each panel. This figure is representative of immunoblot analyses of multiple subcellular fractions generated as previously described [9].

by apoptosis, the loss of plasma membrane integrity over extended periods implied a secondary necrosis phenomenon (Fig. 1). The progressive development of cellular damage *in vitro* over 24–72 hr was also consistent with clinical observations. Thus, the TAMH cell line may represent a good culture model for the bioactivation of APAP and may also have applicability to studies with other toxicants requiring CYP-mediated bioactivation.

Nuclear morphology and DNA fragmentation of TAMH cultures were examined in an effort to determine the type of cell death produced by APAP. These data were compared to effects on TAMH cells treated with the nonhepatotoxic AMAP isomer or proapoptotic act.D/TNFα. Considerable chromatin margination was evident with either of the two structural isomers, although complete chromatin collapse was characteristic of APAP treatment only (Fig. 2A). The incidence of chromatin condensation was qualitatively increased with low concentrations of MG132 (100–250 nM, Fig. 2). Although MG132 treatment *per se* was indistinguishable from control cultures, coincubation in the presence of APAP or AMAP substantially increased chromatin margination and, especially, complete nuclear condensation. These qualitative assessments, necessitated by the amount of cell death found in combined APAP/AMAP/MG132 treatments, implied that the otherwise subtoxic levels of MG132 may exacerbate injury by further inhibition of an APAP target protein, the proteasome.

Changes in chromatin structure corresponded well with APAP-induced DNA fragmentation to *ca.* 50 kbp fragments *in vitro* as determined by CHEF gel electrophoresis. DNA fragmentation was also detected *in vivo*, although there were some differences apparent between the *in vitro* and *in vivo* systems (compare panel E of Fig. 2 with panels B and C). Furthermore, despite previous reports, *in vivo* or *in vitro* oligosomal laddering was not evident with APAP or AMAP even in the presence of high mass DNA fragmentation, supporting the opinion that internucleosomal DNA cleavage, although common, is dispensable [48,49]. Previous studies have shown that higher mass fragmentation is a prerequisite for oligosomal and 50 kbp formation and thus represents an early stage of apoptotic heterochromatin cleavage [50]. Consequently, 50 kbp fragment formation in TAMH cells following APAP or AMAP treatment may likely represent a more terminal stage of apoptotic nuclear degradation. An intriguing possibility, which requires further work, is that CAD/DFF40 is the previously unidentified nuclease in APAP-mediated cell death. As CAD activity appears not to be required for the formation of high mass DNA fragments, however, APAP and AMAP treatments may either partially inhibit CAD activity *per se* or another fragmentation mechanism may be responsible (i.e. 'Stage I' apoptosis via apoptosis inducing factor, AIF; [51,52]).

An up-regulation of ATF3 protein in response to APAP treatment in the TAMH cell line confirms previous *in vivo* studies [37] and also appeared to correlate well with the predicted cytotoxic potencies of these two isomers (Fig. 3A). The apparent correlation with cytotoxic potency was even more evident when the protein levels of the downstream ATF3 target gene, *GADD153*, were considered (Fig. 3). It is interesting to note that a mechanistic link has been defined recently between increased GADD153 levels and the induction of apoptosis by down-regulation of anti-apoptotic BCL-2 protein [53]. In any event, to the best of our knowledge, this represents the only *in vitro* cell line that discriminates between these two isomers of acetaminophen.

An absence of caspase-3 activation, and ultimately deregulation of the conventional apoptotic caspase cascade, was evident during both APAP and AMAP treatments. Specifically, we were unable to detect processing of procaspase-3 into mature forms in any of the *in vitro* or *in vivo* treatment regimens (Figs. 4 and 7). In addition, TAMH cultures treated with a *bona fide* apoptotic regimen (act.D/TNFα) resulted in increased caspase activities at least an order of magnitude higher than with APAP treatment (Fig. 5). As a result, the biological significance of Ac-DEVD-amc cleavage during APAP treatment of TAMH is conjectural and may just represent an induction of alternate caspase-3-like activities with overlapping cleavage capacities, e.g. caspase-7 [44]. APAP-mediated TAMH cell death was also not inhibited by the addition of the broad range caspase inhibitor Z-Val-Ala-Asp-fluoromethyketone (50 μM, data not presented). Finally, we

observed a comparatively low induction of caspase activity in mice after APAP or AMAP treatment (Fig. 5), supporting other reports which have failed to detect Ac-DEVD-amc cleavage after APAP treatment *in vivo* [54,55]. Consequently, APAP- or AMAP-mediated cell killing appears not to be predominantly caspase-3 driven. For APAP, at least, this may represent a product of the lowering of cellular ATP and dATP levels [15,56] or HSP70-directed inhibition of APAF1 (see below).

Recently, an extensive analysis of mouse proteins arylated by NAPQI after APAP and AMAP dosing was undertaken [12,57]. Combined with previous studies (for reviews see Refs. [6–8]), the majority of modified cellular proteins have now been identified. Studies such as these provide the basis for determining the mechanism of cell death via APAP-mediated alterations to the normal function of critical protein(s). We therefore examined protein degradation phenomena as the proteasome represents the only cellular proteolytic activity known to be arylated during APAP treatment [12]. Our findings indicate that the catabolic degradation of proteins during APAP-mediated TAMH cell death *in vitro* is widespread but not universal (Fig. 4). As predicted by other studies [12], we observed an inhibition of both *in vitro* and *in vivo* proteasomal activity (Fig. 5B and C), thereby confirming that the proteasome represents a physiologically significant target for APAP-mediated protein adduction and consequent cell death. In comparison, proteasomal activity was not inhibited during act.D/TNFα treatment, thereby distinguishing it from APAP-mediated cell death (Fig. 5).

The proteasome represents the major pathway for degradation of normal and abnormal proteins within the cell [58,59]. As a result, these data have clear implications for the mechanism of APAP-mediated cell death. Nonetheless, other cellular proteolytic activities (e.g. TPPII and/or calpains) may compensate for APAP-mediated inhibitory effects on caspase and proteasome activities and warrant further investigation. It is of interest to note, however, that proteasomal inhibition has been shown previously to limit caspase-3 activation, PARP processing, and ultimately to induce apoptosis in other cell types [60,61].

Evidence from numerous sources implicates the mitochondrion as a critical site in the ultimate development of cell death after APAP treatment. For example, only after selective depletion of mitochondrial glutathione pools does AMAP treatment result in the covalent modification of mitochondrial proteins, an altered mitochondrial biochemistry, and hepatotoxicity [14,15]. Likewise, although many potentially important mitochondrial proteins are arylated by APAP [12], using identical experimental conditions none are covalently modified by AMAP [57]. Coupled with the pivotal role that mitochondria play in controlling apoptosis, it was of importance to examine alterations to this organelle during APAP- and AMAP-mediated cell death. Previously we have shown a BAX-associated release of mitochondrial cytochrome *c* early after APAP treatment *in vivo* and that these events coincide with increases in as yet undefined cellular proteolytic capacities [25]. In addition to BAX, a proapoptotic member of the BCL-2 family, other proapoptotic proteins also seem to play a role in APAP-mediated cell death both *in vitro* and *in vivo* (e.g. ICAD, Figs. 4 and 7). Moreover, apparent increases in mitochondrial number resulting from APAP exposure are reminiscent of increased mitochondrial fission found more generally during apoptosis [62,63]. Despite these clear mitochondrial changes, cellular caspase activities do not seem to be a hallmark of APAP- or AMAP-induced cell death. The most likely explanation would appear to be an induction of HSP70 by APAP [64] and downstream inhibition of APAF1/procaspase-9 [65,66].

In summary, the complex cellular events seen after APAP and AMAP exposure are distinctive and retain some characteristics of apoptosis. In contrast to more commonly observed apoptotic cell death (e.g. act.D/TNFα), APAP- and AMAP-induced cell death resembles cell death intermediate between apoptosis and necrosis. The proteasome is also implicated in the differential cytotoxic potencies of APAP and AMAP and may play an important role in drug-induced cell death via interrelationships with various cellular compartments. Finally, our findings suggest that the clinical usefulness of AMAP as an analgesic will be limited in situations of concurrent proteasomal inhibition, e.g. during HIV drug therapy [67], as the likelihood of adverse affects will increase.

Acknowledgments

We are grateful to Drs. Anja van Brabant for assistance with CHEF gel analyses and Cathy Lazaro for TAMH cell culture advice. We also appreciate the help of Audrey Wass for EM studies and Lisa Pritchard for immunoblot analyses of TAMH cultures. We would also like to thank Drs. K. Samejima and W. Earnshaw (University of Edinburgh) for antisera to ICAD, and D.W. Nicholson (Merck) for caspase-3 antibody. We thank Dr. Terry Kavanagh for helpful advice and constant encouragement. This work was supported by NIH Grants GM51916 to S.A.B., CA74131 to N.F., GM25418 to S.D.N., and by NIEHS Center Grant P30ES07033.

References

[1] Prescott LF. Paracetamol (acetaminophen): a critical bibliographic review. London: Taylor & Francis, 1996.
[2] Nelson EB, inventor U.S. Patent 4,238,508, assignee. Analgesia using 3-hydroxyacetanilide. USA 1981.
[3] Baker JA, Hayden J, Marshall PG, Palmer CHR, Whittet TD. Some antipyretics related to aspirin and phenacetin. J Pharm Pharmacol 1963;15:97T–100T.
[4] Nelson EB. The pharmacology and toxicology of meta-substituted acetanilide I: acute toxicity of 3-hydroxyacetanilide in mice. Res Commun Chem Pathol Pharmacol 1980;28:447–56.

[5] Jollow DJ, Mitchell JR, Potter WZ, Davis DC, Gillette JR, Brodie BB. Acetaminophen-induced hepatic necrosis. II. Role of covalent binding *in vivo*. J Pharmacol Exp Ther 1973;187:195–202.
[6] Bessems JG, Vermeulen NP. Paracetamol (acetaminophen)-induced toxicity: molecular and biochemical mechanisms, analogues and protective approaches. Crit Rev Toxicol 2001;31:55–138.
[7] Nelson SD, Bruschi SA. Mechanisms of acetaminophen-induced liver disease. In: Kaplowitz N, DeLeve LD, editors. Drug-induced liver disease. New York: Marcel Dekker, in press.
[8] Pumford NR, Halmes NC. Protein targets of xenobiotic reactive intermediates. Annu Rev Pharmacol Toxicol 1997;37:91–117.
[9] Tonge RP, Kelly EJ, Bruschi SA, Kalhorn T, Eaton DL, Nebert DW, Nelson SD. Role of CYP1A2 in the hepatotoxicity of acetaminophen: investigations using *Cyp1a2* null mice. Toxicol Appl Pharmacol 1998;153:102–8.
[10] Zaher H, Buters JTM, Ward JM, Bruno MK, Lucas AM, Stern ST, Cohen SD, Gonzalez FJ. Protection against acetaminophen toxicity in CYP1A2 and CYP2E1 double-null mice. Toxicol Appl Pharmacol 1998;152:193–9.
[11] Chen W, Koenigs LL, Thompson SJ, Peter RM, Rettie AE, Trager WF, Nelson SD. Oxidation of acetaminophen to its toxic quinone imine and nontoxic catechol metabolites by baculovirus-expressed and purified human cytochromes P450 2E1 and 2A6. Chem Res Toxicol 1998;11: 295–301.
[12] Qiu Y, Benet LZ, Burlingame AL. Identification of the hepatic protein targets of reactive metabolites of acetaminophen *in vivo* in mice using two-dimensional gel electrophoresis and mass spectrometry. J Biol Chem 1998;273:17940–53.
[13] Vendemiale G, Grattagliano I, Altomare E, Turturro N, Guerrieri F. Effect of acetaminophen administration on hepatic glutathione compartmentation and mitochondrial energy metabolism in the rat. Biochem Pharmacol 1996;52:1147–54.
[14] Tirmenstein MA, Nelson SD. Hepatotoxicity after 3′-hydroxyacetanilide administration to buthionine sulfoximine pretreated mice. Chem Res Toxicol 1991;4:214–7.
[15] Tirmenstein MA, Nelson SD. Acetaminophen-induced oxidation of protein thiols. Contribution of impaired thiol-metabolizing enzymes and the breakdown of adenine nucleotides. J Biol Chem 1990;265: 3059–65.
[16] Moore M, Thor H, Moore G, Nelson S, Moldéus P, Orrenius S. The toxicity of acetaminophen and *N*-acetyl-*p*-benzoquinone imine in isolated hepatocytes is associated with thiol depletion and increased cytosolic Ca^{2+}. J Biol Chem 1985;260:13035–40.
[17] Bruschi SA, Priestly BG. Implications of alterations in intracellular calcium ion homeostasis in the advent of paracetamol-induced cytotoxicity in primary mouse hepatocyte cultures. Toxicol In Vitro 1990;4:743–9.
[18] Tirmenstein MA, Nelson SD. Subcellular binding and effects on calcium homeostasis produced by acetaminophen and a nonhepatotoxic regioisomer, 3′-hydroxyacetanilide, in mouse liver. J Biol Chem 1989;264:9814–9.
[19] Nakae D, Yamamoto K, Yoshiji H, Kinugasa T, Maruyama H, Farber JL, Konishi Y. Liposome-encapsulated superoxide dismutase prevents liver necrosis induced by acetaminophen. Am J Pathol 1990;136:787–95.
[20] Smith CV, Mitchell JR. Acetaminophen hepatotoxicity *in vivo* is not accompanied by oxidant stress. Biochem Biophys Res Commun 1985;133:329–36.
[21] Mirochnitchenko O, Weisbrot-Lefkowitz M, Reuhl K, Chen L, Yang C, Inouye M. Acetaminophen toxicity. Opposite effects of two forms of glutathione peroxidase. J Biol Chem 1999;274:10349–55.
[22] Cohen SD, Pumford NR, Khairallah EA, Boekelheide K, Pohl LR, Amouzadeh HR, Hinson JA. Selective protein covalent binding and target organ toxicity. Toxicol Appl Pharmacol 1997;143:1–12.
[23] Henderson CJ, Wolf CR, Kitteringham N, Powell H, Otto D, Park BK. Increased resistance to acetaminophen hepatotoxicity in mice lacking glutathione *S*-transferase Pi. Proc Natl Acad Sci USA 2000;97:12741–5.
[24] Rzucidlo SJ, Bounous DI, Jones DP, Brackett BG. Acute acetaminophen toxicity in transgenic mice with elevated hepatic glutathione. Vet Hum Toxicol 2000;42:146–50.
[25] Adams ML, Pierce RH, Vail ME, White CC, Tonge RP, Kavanagh TJ, Fausto N, Nelson SD, Bruschi SA. Enhanced acetaminophen hepatotoxicity in transgenic mice overexpressing BCL-2. Mol Pharmacol 2001;60:907–15.
[26] Wu JC, Merlino G, Cveklova K, Mosinger Jr B, Fausto N. Autonomous growth in serum-free medium and production of hepatocellular carcinomas by differentiated hepatocyte lines that overexpress transforming growth factor α. Cancer Res 1994;54:5964–73.
[27] Franklin CC, Srikanth S, Kraft AS. Conditional expression of mitogen-activated protein kinase phosphatase-1, MKP-1, is cytoprotective against UV-induced apoptosis. Proc Natl Acad Sci USA 1998;95: 3014–9.
[28] Tsubuki S, Kawasaki H, Saito Y, Miyashita N, Inomata M, Kawashima S. Purification and characterization of a Z-Leu-Leu-Leu-MCA degrading protease expected to regulate neurite formation: a novel catalytic activity in proteasome. Biochem Biophys Res Commun 1993;196:1195–201.
[29] Wu JC, Merlino G, Fausto N. Establishment and characterization of differentiated, nontransformed hepatocyte cell lines derived from mice transgenic for transforming growth factor α. Proc Natl Acad Sci USA 1994;91:674–8.
[30] Fischer LJ, Green MD, Harman AW. Studies on the fate of the glutathione and cysteine conjugates of acetaminophen in mice. Drug Metab Dispos 1985;13:121–6.
[31] Fischer LJ, Green MD, Harman AW. Levels of acetaminophen and its metabolites in mouse tissues after a toxic dose. J Pharmacol Exp Ther 1981;219:281–6.
[32] Ray SD, Kamendulis LM, Gurule MW, Yorkin RD, Corcoran GB. Ca^{2+} antagonists inhibit DNA fragmentation and toxic cell death induced by acetaminophen. FASEB J 1993;7:453–63.
[33] Ray SD, Mumaw VR, Raje RR, Fariss MW. Protection of acetaminophen-induced hepatocellular apoptosis and necrosis by cholesteryl hemisuccinate pretreatment. J Pharmacol Exp Ther 1996;279: 1470–83.
[34] Malek NP, Sundberg H, McGrew S, Nakayama K, Kyriakidis TR, Roberts JM, Kyriakidis TR. A mouse knock-in model exposes sequential proteolytic pathways that regulate $p27^{Kip1}$ in G1 and S phase. Nature 2001;413:323–7.
[35] Kreuz S, Siegmund D, Scheurich P, Wajant H. NF-κB inducers upregulate cFLIP, a cycloheximide-sensitive inhibitor of death receptor signaling. Mol Cell Biol 2001;21:3964–73.
[36] Asher G, Lotem J, Cohen B, Sachs L, Shaul Y. Regulation of p53 stability and p53-dependent apoptosis by NADH quinone oxidoreductase 1. Proc Natl Acad Sci USA 2001;98:1188–93.
[37] Hai T, Wolfgang CD, Marsee DK, Allen AE, Sivaprasad U. ATF3 and stress responses. Gene Expr 1999;7:321–35.
[38] Chen BPC, Wolfgang CD, Hai T. Analysis of ATF3, a transcription factor induced by physiological stresses and modulated by gadd153/ Chop10. Mol Cell Biol 1996;16:1157–68.
[39] Wolfgang CD, Chen BPC, Martindale JL, Holbrook NJ, Hai T. *gadd153/Chop10*, a potential target gene of the transcriptional repressor ATF3. Mol Cell Biol 1997;17:6700–7.
[40] Fawcett TW, Martindale JL, Guyton KZ, Hai T, Holbrook NJ. Complexes containing activating transcription factor (ATF)/cAMP-responsive-element-binding protein (CREB) interact with the CCAAT/ enhancer-binding protein (C/EBP)-ATF composite site to regulate *Gadd153* expression during the stress response. Biochem J 1999; 339:135–41.
[41] Enari M, Sakahira H, Yokoyama H, Okawa K, Iwamatsu A, Nagata S. A caspase-activated DNase that degrades DNA during apoptosis, and its inhibitor ICAD. Nature 1998;391:43–50.
[42] Zhang J, Liu X, Scherer DC, van Kaer L, Wang X, Xu M. Resistance to DNA fragmentation and chromatin condensation in mice lacking the

DNA fragmentation factor 45. Proc Natl Acad Sci USA 1998;95: 12480–5.
[43] Shah GM, Shah RG, Poirier GG. Different cleavage pattern for poly(ADP-ribose) polymerase during necrosis and apoptosis in HL-60 cells. Biochem Biophys Res Commun 1996;229:838–44.
[44] Thornberry NA, Rano TA, Peterson EP, Rasper DM, Timkey T, Garcia-Calvo M, Houtzager VM, Nordstrom PA, Roy S, Vaillancourt JP, Chapman KT, Nicholson DW. A combinatorial approach defines specificities of members of the caspase family and granzyme B. Functional relationships established for key mediators of apoptosis. J Biol Chem 1997;272:17907–11.
[45] Yoshitomi S, Ikemoto K, Takahashi J, Miki H, Namba M, Asahi S. Establishment of the transformants expressing human cytochrome P450 subtypes in HepG2 and their applications on drug metabolism and toxicology. Toxicol In Vitro 2001;15:245–56.
[46] Dai Y, Cederbaum AI. Cytotoxicity of acetaminophen in human cytochrome P4502E1-transfected HepG2 cells. J Pharmacol Exp Ther 1995;273:1497–505.
[47] Thummel KE, Lee CA, Kunze KL, Nelson SD, Slattery JT. Oxidation of acetaminophen to *N*-acetyl-*p*-aminobenzoquinone imine by human CYP3A4. Biochem Pharmacol 1993;45:1563–9.
[48] Schulze-Osthoff K, Walczak H, Droge W, Krammer PH. Cell nucleus and DNA fragmentation are not required for apoptosis. J Cell Biol 1994;127:15–20.
[49] Oberhammer F, Wilson JW, Dive C, Morris ID, Hickman JA, Wakeling AE, Walker PR, Sikorska M. Apoptotic death in epithelial cells: cleavage of DNA to 300 and/or 50 kb fragments prior to or in the absence of internucleosomal fragmentation. EMBO J 1993;12:3679–84.
[50] Brown DG, Sun XM, Cohen GM. Dexamethasone-induced apoptosis involves cleavage of DNA to large fragments prior to internucleosomal fragmentation. J Biol Chem 1993;268:3037–9.
[51] Samejima K, Tone S, Earnshaw WC. CAD/DFF40 nuclease is dispensable for high molecular weight DNA cleavage and stage I chromatin condensation in apoptosis. J Biol Chem 2001;276:45427–32.
[52] Susin SA, Daugas E, Ravagnan L, Samejima K, Zamzami N, Loeffler M, Costantini P, Ferri KF, Irinopoulou T, Prevost MC, Brothers G, Mak TW, Penninger J, Earnshaw WC, Kroemer G. Two distinct pathways leading to nuclear apoptosis. J Exp Med 2000;192:571–80.
[53] McCullough KD, Martindale JL, Klotz L-O, Aw T-Y, Holbrook NJ. Gadd153 sensitizes cells to endoplasmic reticulum stress by down-regulating Bcl2 and perturbing the cellular redox state. Mol Cell Biol 2001;21:1249–59.
[54] Lawson JA, Fisher MA, Simmons CA, Farhood A, Jaeschke H. Inhibition of Fas receptor (CD95)-induced hepatic caspase activation and apoptosis by acetaminophen in mice. Toxicol Appl Pharmacol 1999;156:179–86.
[55] Hentze H, Gantner F, Kolb SA, Wendel A. Depletion of hepatic glutathione prevents death receptor-dependent apoptotic and necrotic liver injury in mice. Am J Pathol 2000;156:2045–56.
[56] Leist M, Single B, Castoldi AF, Kuhnle S, Nicotera P. Intracellular adenosine triphosphate (ATP) concentration: a switch in the decision between apoptosis and necrosis. J Exp Med 1997;185:1481–6.
[57] Qiu Y, Benet LZ, Burlingame AL. Identification of hepatic protein targets of the reactive metabolites of the non-hepatotoxic regioisomer of acetaminophen, 3′-hydroxyacetanilide, in the mouse *in vivo* using two-dimensional gel electrophoresis and mass spectrometry. Adv Exp Med Biol 2001;500:663–73.
[58] Rock KL, Gramm C, Rothstein L, Clark K, Stein R, Dick L, Hwang D, Goldberg AL. Inhibitors of the proteasome block the degradation of most cell proteins and the generation of peptides presented on MHC class I molecules. Cell 1994;78:761–71.
[59] Schubert U, Anton LC, Gibbs J, Norbury CC, Yewdell JW, Bennink JR. Rapid degradation of a large fraction of newly synthesized proteins by proteasomes. Nature 2000;404:770–4.
[60] Sadoul R, Fernandez PA, Quiquerez AL, Martinou I, Maki M, Schroter M, Becherer JD, Irmler M, Tschopp J, Martinou JC. Involvement of the proteasome in the programmed cell death of NGF-deprived sympathetic neurons. EMBO J 1996;15:3845–52.
[61] Grimm LM, Goldberg AL, Poirier GG, Schwartz LM, Osborne BA. Proteasomes play an essential role in thymocyte apoptosis. EMBO J 1996;15:3835–44.
[62] Frank S, Gaume B, Bergmann-Leitner ES, Leitner WW, Robert EG, Catez F, Smith CL, Youle RJ. The role of dynamin-related protein 1, a mediator of mitochondrial fission, in apoptosis. Dev Cell 2001;1: 515–25.
[63] Mancini M, Anderson BO, Caldwell E, Sedghinasab M, Paty PB, Hockenbery DM. Mitochondrial proliferation and paradoxical membrane depolarization during terminal differentiation and apoptosis in a human colon carcinoma cell line. J Cell Biol 1997;138:449–69.
[64] Salminen WF, Voellmy R, Roberts SM. Effect of N-acetylcysteine on heat shock protein induction by acetaminophen in mouse liver. J Pharmacol Exp Ther 1998;286:519–24.
[65] Beere HM, Wolf BB, Cain K, Mosser DD, Mahboubi A, Kuwana T, Tailor P, Morimoto RI, Cohen GM, Green DR. Heat-shock protein 70 inhibits apoptosis by preventing recruitment of procaspase-9 to the Apaf-1 apoptosome. Nat Cell Biol 2000;2:469–75.
[66] Saleh A, Srinivasula SM, Balkir L, Robbins PD, Alnemri ES. Negative regulation of the Apaf-1 apoptosome by Hsp70. Nat Cell Biol 2000; 2:476–83.
[67] Schmidtke G, Holzhutter HG, Bogyo M, Kairies N, Groll M, de Giuli R, Emch S, Groettrup M. How an inhibitor of the HIV-I protease modulates proteasome activity. J Biol Chem 1999;274:35734–40.